RESEARCH ARTICLE

Check for updates

Near-infrared-photoinduced metamagnet based on a layered cyanido-bridged Co−W assembly with π−π interactions†

Kazuki Nakamura,[a,b] Koji Nakabayashi, ✉ *[a,b] Shota Kobayashi[a] and Shin-ichi Ohkoshi ✉ *[a,b]

A newly synthesized photomagnet based on a cyanido-bridged Co−W assembly, [{Co(isoquinoline)$_4$}$_3${W(CN)$_8$}$_2$]·2EtOH (**CoWisoq**), exhibits a controllable photoinduced (PI) phase with a metamagnetic behavior. The PI phase shows a transition from paramagnetic to ferromagnetic with a coercive field of 550 Oe at 2 K. It has a monoclinic ($P2_1/n$) crystal structure and is comprised of two-dimensional cyanido-bridged Co−W coordination layers with two crystallographically independent Co sites (Co1, Co2) and one W site. Both Co sites adopt a pseudo-octahedral six-coordinated geometry involving four isoquinoline and two cyanide ligands. π−π interactions are induced at half of the isoquinoline ligands in Co1 and all of those in Co2 sites, suggesting that the coordination environment at the Co1 site has structural flexibility. **CoWisoq** displays a thermal phase transition around 140 K with a small thermal hysteresis due to the charge transfer−induced spin transition between Co^{II}−W^V of the high temperature (HT) phase and Co^{III}−W^{IV} of the low temperature (LT) phase. This charge transfer, which is also responsible for a drastic color change between purple (HT) and yellow (LT), involves only the structurally flexible Co1 sites. The ligand field, which is composed of four isoquinoline and two cyanide ligands, contributes to a unique metal-to-metal charge transfer absorption band of the LT phase at 1025 nm. Irradiation of the LT phase with near−infrared light produces a PI phase with the Co^{II}−W^V state.

Introduction

Molecule-based magnets[1–15] have been widely investigated because of versatile interesting functionalities by the combination of the components of metal ions, organic ligands, and crystalline solvent molecules.[16–28] In particular, cyanido-bridged bimetal assemblies show a high structural designability and diverse physical properties *e.g.*, barocaloric effect,[29] low-frequency THz wave absorption,[30] ionic conductivity.[31] Octacyanidemetallates are good building blocks due to the variety of coordination geometries, including square antiprism, bicapped trigonal prism, and dodecahedron, and have a high coordination number. These characteristics realize various dimensional coordination structures and physical properties.[32–35]

Appropriate combinations of redox-active transition metal ions and octacyanidotungstate with the redox activity between W^V (S = 1/2) and W^{IV} (S = 0) produce charge-transfer (CT) phase transition compounds. For example, cyanido-bridged Co–W assemblies exhibit a phase transition between the high temperature (HT) phase with a Co^{II}–W^V state and the low temperature (LT) phase with a Co^{III}–W^{IV} state. Some cyanido-bridged Co–W assemblies display interesting features such as thermal phase transitions with thermal hysteresis loops or photoinduced (PI) magnetization based on CT-induced spin transitions.[36–40]

Photomagnetic behavior is initiated by CT from W^{IV} to Co^{III} to produce the low-spin Co^{II} state and subsequent spin transition to the high-spin Co^{II} state. The wavelength used for the PI phase transition depends on the energy band of metal-to-metal charge transfer (MMCT) between the Co and W sites. MMCT usually occurs around 700–800 nm[37–40] due to the similarity of their ligand field splitting on the Co sites provided by the four nitrogen atoms of the cyanide ligands in the equatorial position and the two nitrogen atoms of organic ligands in the axial position. In Co–W photomagnet systems, substitutions of the organic ligands may control the MMCT absorp-

[a]Department of Chemistry, School of Science, The University of Tokyo, 7-3-1, Hongo, Bunkyo-ku, Tokyo 113-0033, Japan. E-mail: ohkoshi@chem.s.u-tokyo.ac.jp
[b]DYNACOM IRL2015 University of Tokyo - CNRS - Universite de Rennes, Department of Chemistry, 7-3-1, Hongo, Bunkyo-ku, Tokyo 113-0033, Japan
†Electronic supplementary information (ESI) available: Product characterization of optical and single-crystal XRD data and optical, magnetic, and photomagnetic studies. CCDC 2331970–2331972. For ESI and crystallographic data in CIF or other electronic format see DOI: https://doi.org/10.1039/d4qi00511b

2752 | *Inorg. Chem. Front.*, 2024, **11**, 2752–2762

This journal is © the Partner Organisations 2024

tion band as it changes the ligand field splitting and coordination geometries.[41–44] Furthermore, alternating the organic ligands should also affect the thermal and PI phase transitions based on a CT-induced spin transition because it not only modulates the MMCT band but also alters intermolecular interactions.[45,46]

Our research focuses on a slightly large aromatic ligand of isoquinoline (isoq) to control the photomagnetic properties of the Co–W system. Isoq should realize more effective intermolecular π–π interactions[47–49] than pyridine, pyrimidine, and their previously reported derivatives.[37,39] In this study, we synthesize a two-dimensional cyanido-bridged Co–W assembly with a near-infrared MMCT absorption band, [{Co(isoq)$_4$}$_3${W(CN)$_8$}$_2$]·2EtOH (**CoWisoq**). **CoWisoq** exhibits PI magnetization by near–infrared light irradiation. Its PI phase shows metamagnetism because the deliberate introduction of isoq causes π–π interactions. Herein we report its crystal structure, thermal phase transition, optical properties, photomagnetism, and PI metamagnetism.

Results and discussion

Synthesis and crystal structure

A purple crystal of **CoWisoq** was obtained by the slow diffusion method and kept for 2–3 weeks by adding a mixed solution of ethanol and water containing CoCl$_2$·6H$_2$O and isoq into an aqueous solution of Cs$_3$[W(CN)$_8$]·2H$_2$O at room temperature. Elemental analyses by inductively coupled plasma mass spectrometry (ICP-MS) for metal ions, standard method for C, H, and N, and thermogravimetry (TG) measurement revealed that the composition of the present compound is [{Co(isoq)$_4$}$_3${W(CN)$_8$}$_2$]·2EtOH. A single crystal X-ray diffraction (XRD) measurement at 300 K indicated that this compound is monoclinic in the $P2_1/n$ space group (a = 14.6601(4) Å, b = 27.5666(5) Å, c = 15.3341(4) Å, β = 112.706(3)°) (Fig. 1, S4, Table S1†). The asymmetric unit of **CoWisoq** is composed of a [W^V(CN)$_8$]$^{3-}$ anion, a [Co(isoq)$_4$]$^{2+}$ cation (Co1), one-half of [Co(isoq)$_4$]$^{2+}$ cation (Co2), and an EtOH molecule.
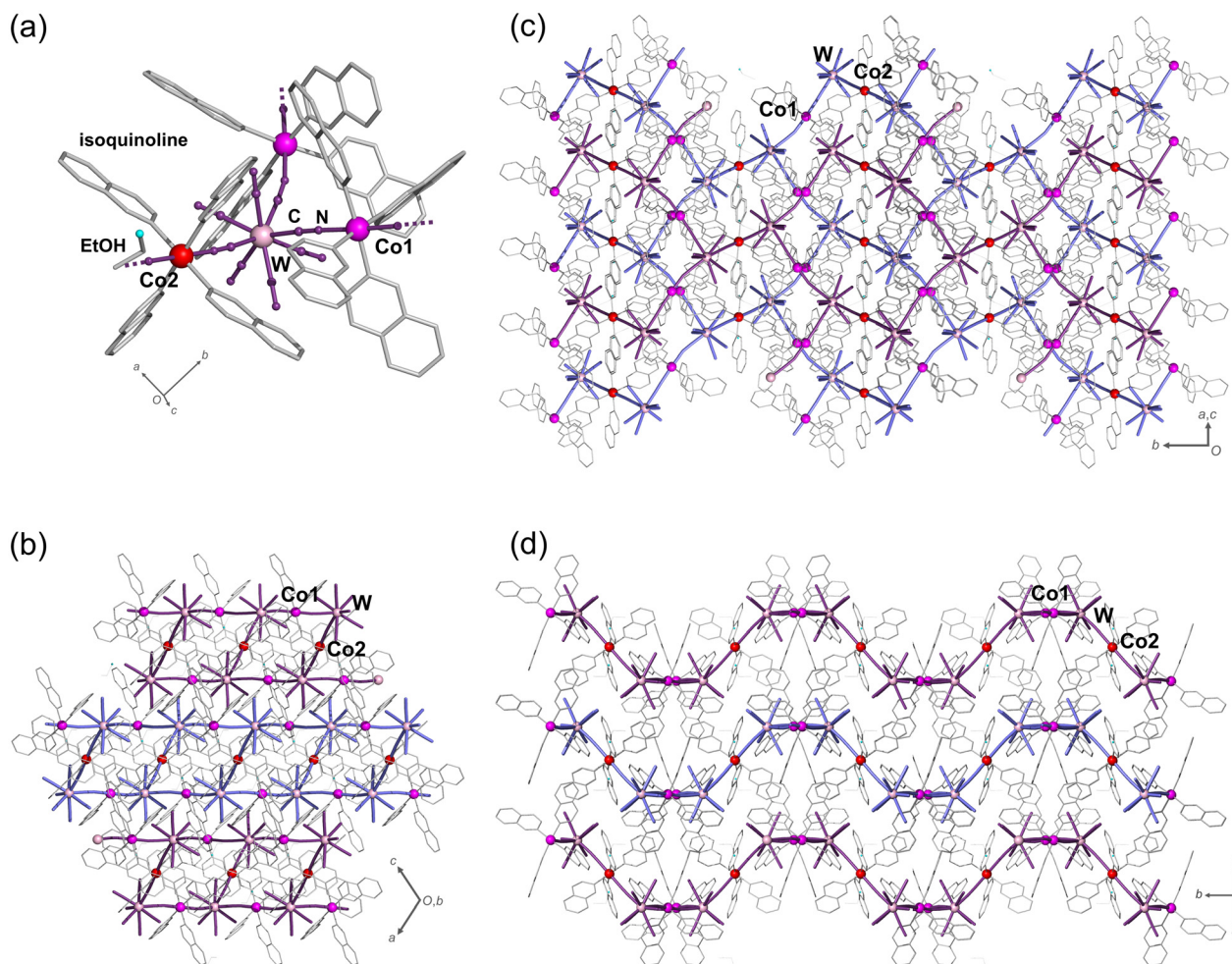

Fig. 1 Crystal structure of **CoWisoq** at 300 K. (a) Coordination environment of **CoWisoq**. Purple, red, pink, and light blue spheres and the gray line indicate Co1, Co2, W, O, and isoq ligands, respectively. Packing structure of **CoWisoq** viewed from (b) the *b*-axis, (c) the (10−1) plane, and (d) the (101) plane. Purple and blue thick lines represent the first (and third) layer and the second layer of cyanido-bridged coordination networks, respectively.

This journal is © the Partner Organisations 2024

Inorg. Chem. Front., 2024, **11**, 2752–2762 | **2753**

The coordination geometry of the W site is close to that of an ideal dodecahedron (Table S2†). The three cyanide groups of $[W(CN)_8]^{3-}$ are connected to three Co atoms (two Co1 and one Co2). The remaining groups are terminal. The Co1 and Co2 sites adopt a pseudo-octahedral six-coordinated geometry, which is occupied by four nitrogen atoms of isoq ligands in equatorial positions and two nitrogen atoms of $[W(CN)_8]^{3-}$ in axial positions. The cyanido-bridged Co1–W connections create zigzag chains. These chains are bound by the Co2 sites, providing two-dimensional dodecanuclear hexagonal units of cyanido-bridged Co6W6 (4Co1–2Co2–W6) moieties. The two-dimensional layers are displaced from each other and stacked along the [101] direction. A non-coordinated EtOH molecule is in the interstitial site (central part) of the hexagonal units. The single crystal left in the air for more than one year still has the EtOH molecules in the crystal structure. The distance between the layers in the [10−1] direction is 12.47 Å, and the nearest W–W and Co–Co distances between the layers are 10.12 Å and 11.89 Å, respectively (Fig. S5†).

The four isoq ligands of the Co2 site realize π–π interactions with isoq ligands of the Co1 sites in the same layer and in the neighboring layer with arene–arene distances of 3.67 Å and 3.94 Å, respectively (Fig. 2, S7, Table S3†).[50,51] The displacement angles formed between the ring-centroid vector and the pyridine-ring plane are at 17.47° within the layer and 15.94° between the layers (Table S4†). These π–π interactions may stabilize the crystal structure, including the characteristic coordination environment with four pyridine-based ligands (isoq) coordinated to the Co site. This is a representative structural feature of **CoWisoq** and differs from cyanido-bridged Co–W assemblies in which two pyridine-analogue ligands coordinate to the Co site.[30,38] The Co–N distances are 2.10–2.18 Å for Co1–N and 2.12–2.21 Å for Co2–N, indicating that Co1 and Co2 have divalent states (Table S5†). The powder XRD

measurement showed that the powder form has an identical crystal structure to that obtained by the single-crystal X-ray structural analysis (Fig. S9†).

Magnetic properties

The temperature (T) dependence of the molar magnetic susceptibility (χ_M) and T of **CoWisoq** indicated a thermal phase transition with the small thermal hysteresis loop (Fig. 3). The $\chi_M T$ value of 8.46 cm³ K mol⁻¹ at 300 K corresponds well with the expected value of 8.52 cm³ K mol⁻¹ for $Co^{II}_{hs3}W^V_2$ (Co^{II}_{hs}: high spin): $g = 2.35$, $S_{Co} = 3/2$, W^V: $g_W = 2.00$, $S_W = 1/2$), and is denoted as the high temperature (HT) phase. When the temperature decreases to 180 K, the $\chi_M T$ value gradually increases due to spin–orbit coupling in the Co sites and Co^{II}–W^V ferromagnetic coupling in the cyanido-bridged coordination layers.[52–54] From 180 K, the $\chi_M T$ value decreases and reaches 2.58 cm³ K mol⁻¹ at 80 K. This observation agrees with that of 2.59 cm³ K mol⁻¹ for $Co^{III}_{ls2}W^{IV}_2Co^{II}$ (Co^{III}_{ls} (ls: low spin): $S_{Co} = 0$, W^{IV}: $S_W = 0$, Co^{II}: $g = 2.35$, $S_{Co} = 3/2$), named the low temperature (LT) phase, suggesting a CT-induced spin transition. Upon heating, the $\chi_M T$ value for the LT phase is maintained until 140 K, increases sharply around 150 K, and then returns to the value for the HT phase. The transition behaviors with sweep rates of 0.5, 1.0, and 2.0 K min⁻¹ in the $\chi_M T$–T plots are similar, whereas that with 5.0 K min⁻¹ indicates partial quenching of the transition from the HT phase to the LT phase in the cooling process (Fig. S10†). The field-cooled magnetization (FCM) curve does not show a critical temperature, suggesting the LT phase is paramagnetic. The magnetization (M) vs. magnetic-field (H) plot represents the magnetization of the remaining paramagnetic Co^{II} site in the LT phase (Fig. S11†).

Crystal structure of the LT phase

Single crystal XRD analysis of the LT phase of **CoWisoq** at 90 K indicated the same space group of $P2_1/n$ as that at 300 K. The
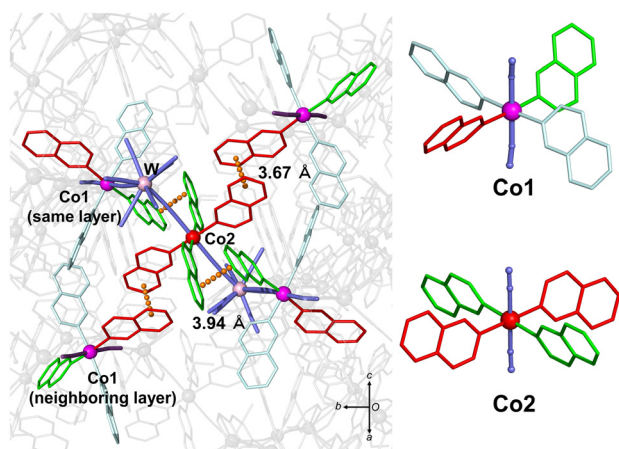

Fig. 2 π–π interactions formed by the isoq ligands coordinated to the Co1 and Co2 sites. Orange dotted lines indicate π–π interactions between the isoq ligands. Red isoq ligands create π–π interactions between the layers, while the green isoq ligands form π–π interactions in the layer. Light blue indicates isoq ligands without π–π interactions. Purple, red, and pink spheres indicate Co1, Co2, and W, respectively.
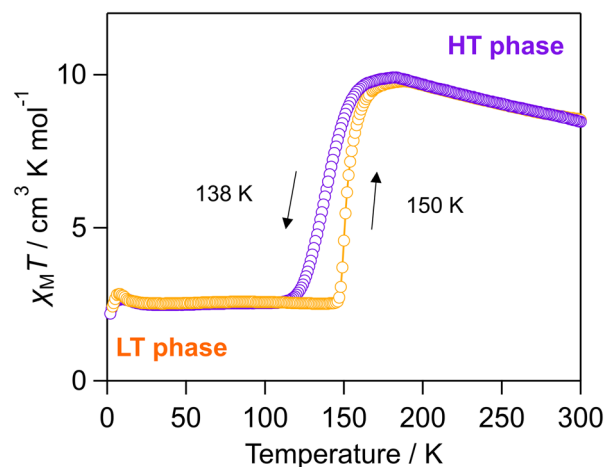

Fig. 3 Temperature dependence of $\chi_M T$ of **CoWisoq** upon cooling (purple) and heating (yellow).

2754 | *Inorg. Chem. Front.*, 2024, **11**, 2752–2762

This journal is © the Partner Organisations 2024

cell parameters are a = 14.3610(4) Å, b = 26.9695(5) Å, c = 15.1714(4) Å, and β = 113.674(3) ° (Fig. S8, Table S1†). The color of the single crystal at 90 K was clear yellow changed from purple for the HT phase (Fig. 4a). The distances of Co–N bonds for Co1 and Co2 sites are 1.90–1.99 Å, and 2.09–2.19 Å, respectively (Table S5†). The Co1–N bond was significantly shortened in comparison with those at 300 K, indicating the valence state of the Co1 site was trivalent at 90 K. By contrast, the Co2–N bond distances are similar to those of the HT phase, indicating that the Co2 site remains in the divalent state.[30,39] Overall, structural analyses and the magnetic susceptibility show that the LT phase of **CoWisoq** has a formula with the electronic state of $[\{Co1^{III}(isoq)_4\}_2\{Co2^{II}(isoq)_4\}\{W^{IV}(CN)_8\}_2]\cdot2EtOH$. The CT-induced spin transition occurs between the Co1 and W sites in the Co1–W zigzag chains (Fig. 4b). The arene–arene distances of the isoq ligands within the layer and between the layers at 90 K become shorter from 3.67 Å and 3.94 Å for the HT phase to 3.54 Å and 3.82 Å for the LT phase, respectively, while arene–arene displacement angles increase from 17.47° to 20.89° within the layer and from 15.94° to 19.63° between the layers (Tables S3 and S4†). Janiak reported that the π–π interactions of pyridine and quinoline systems tend to have a smaller displacement as the distance

decreases, indicating stabilization of the π–π interactions.[51] Therefore, the significant increases of the displacement angles in **CoWisoq** should weaken the π–π interactions in the LT phase. These structural features, especially the π–π interactions, probably affect the CT phase transitions in the cooling and heating processes.

Optical spectroscopy

Variable-temperature UV–vis–NIR absorption spectroscopy confirmed the CT phase transition between the LT and HT phases. At 300 K, **CoWisoq** shows a strong absorption at 530 nm, which is assigned to MMCT from Co^{II} to W^V (Fig. 5, S12†).[37,38,55] In the cooling process, this peak gradually shifts to 550 nm until 160 K, and the intensity significantly decreases around 130 K. Absorption peaks at 500 nm and 1025 nm appear, which are attributed to the d–d transition of Co^{III} and the MMCT from W^{IV} to Co^{III}, respectively. The change of the UV–vis–NIR spectrum corresponds to the color change of the crystal between the LT phase (yellow) and the HT phase (purple).

The LT phases of cyanido-bridged Co–W assemblies reported to date have blue colors due to the MMCT from W^{IV} to Co^{III} in 700–800 nm (Table S6†).[30,36–40] However, **CoWisoq** has a MMCT band of the LT phase at 1025 nm, which is in the infrared light region. The difference of the MMCT absorption band is derived mainly from the ligand field around the Co^{III} site. That is, **CoWisoq** has a ligand field composed of four isoq ligands and two cyanides, while other cyanido-bridged Co–W assemblies have two pyridine analogues and four cyanides coordinated to Co^{III}. Since isoq and pyridine-analogues ligands provide a weaker ligand field than cyanides, the Co sites of **CoWisoq** have smaller ligand field splitting than those of other Co–W assemblies.[41–44] MMCT occurs between the W site and the e_g orbital of the Co site, and the smaller ligand field splitting of the Co site leads to the longer wavelength of the MMCT band. A further red-shift of the MMCT could be possible by using pyridine analogues with weaker ligand field, but the additional shift should be small. Ligands with weaker
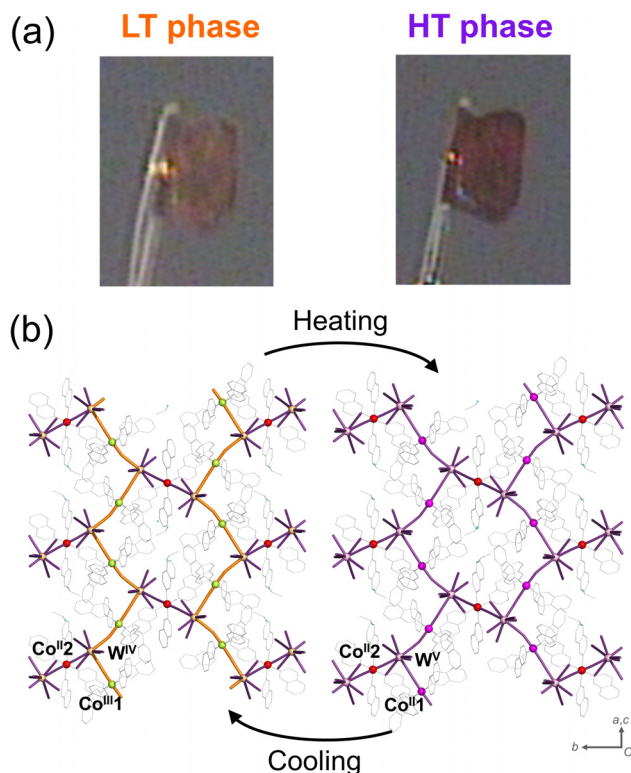

Fig. 4 (a) Photos of a single crystal of **CoWisoq** at 90 K (left) and 300 K (right). (b) Crystal structures of the LT phase at 90 K and the HT phase at 300 K. Purple, red, pink, light green, light yellow, and light blue spheres indicate $Co1^{II}_{hs}$, W^V, $Co2^{II}_{hs}$, $Co1^{III}_{ls}$, W^{IV}, and O, respectively. Purple and yellow thick lines represent the cyanido-bridged network and the $Co1^{III}_{ls}$–W^{IV} zigzag chains, respectively.
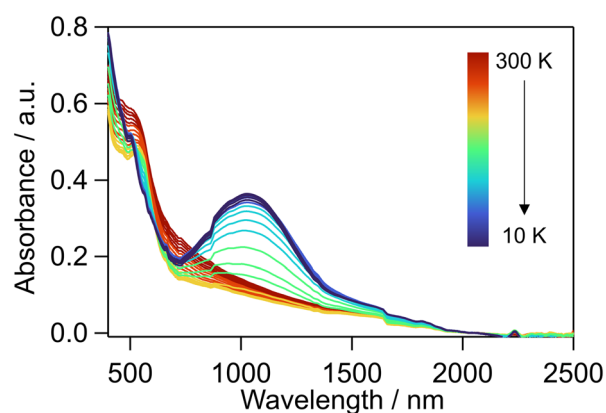

Fig. 5 Variable-temperature UV–vis–NIR absorption spectra of **CoWisoq** upon cooling.

ligand field such as a water molecule and halogen ions would suppress the thermal CT phase transition.[37,54]

Photoinduced phase transition

The photoresponsivity for the LT phase of **CoWisoq** was examined using UV–vis spectroscopy. Irradiation with 980 nm laser light at 3.8 K decreases the MMCT absorption band from W^{IV} to Co^{III} at 1025 nm and increases the MMCT absorption band from Co^{II} to W^{V} at 565 nm (Fig. S13a†). Therefore, the PI phase has the same electronic state of $Co_3^{II}W_2^{V}$ as that of the HT phase. After thermal annealing to 100 K, the MMCT bands at 1025 nm and 565 nm increase and decrease around 70 K (Fig. S13b†), indicating the LT phase is recovered. Further heating to 300 K induces a large decrease in the absorption at 1025 nm and 150 K, which corresponds to the return to the HT phase. In the cooling process, the absorption change traces the temperature dependence of the $\chi_M T$ vs. T plot (Fig. S13c†).

The detailed UV–vis absorption spectra before and after the photoirradiation at 3.8 K contains some peaks. The LT phase before irradiation has absorption peaks at 408, 464, 500, 565, 585, and 662 nm, while the PI phase shows absorption peaks at 464, 565, and 662 nm. The peaks of the PI phase are assigned to d–d transitions of ${}^4E_g \leftarrow {}^4A_{2g}$ (464 nm), ${}^4A_{2g}(P) \leftarrow {}^4A_{2g}(F)$ (565 nm, overlapping with the MMCT), and ${}^4B_{1g} \leftarrow {}^4A_{2g}$ (662 nm) in Co^{II}, considering the coordination geometry of the Co sites with the *trans*-CoX_4Y_2 type (D_{4h}) (X = isoq, Y = cyanide) with longer Co–N distances from isoq ligands than those from cyanides (Fig. S14†).[56–58] In addition to the peaks from the Co^{II} site, the LT phase with both Co^{II} and Co^{III} sites has absorption peaks at 408, 500, and 585 nm, which are attributed to the d–d transitions of to ${}^1E_g^b \leftarrow {}^1A_{1g}$, ${}^1E_g^a \leftarrow {}^1A_{1g}$, and ${}^1A_{2g} \leftarrow {}^1A_{1g}$ in Co^{III}, respectively.[59–61]

The photomagnetic effect of **CoWisoq** was studied by magnetic measurements before and after photoirradiation (Fig. 6, S15†). The LT phase displays a small magnetization value in the FCM curve and the magnetization (M) vs. external magnetic field (H) plots. After irradiation with 980 nm laser light at 3 K under an external magnetic field of 500 Oe, the magnetization value significantly increases below 12 K, suggesting long-range magnetic ordering. In the M–H plots at 2 K, the saturation magnetization value reaches $8.00\mu_B$ at 50 kOe by irradiation (Fig. S15†), and a magnetic hysteresis loop with the coercive field (H_C) of 550 Oe was observed.

The saturation magnetization value of the PI phase is close to $8.50\mu_B$, assuming ferromagnetic interactions between Co^{II} (Kramers doublet: $g = 13/3$, $S_{Co} = 1/2$) and W^V ($g_W = 2.00$, $S_W = 1/2$) for the Co_3W_2 unit rather than that of $4.50\mu_B$ assuming antiferromagnetic interactions. The magnetization value of the PI phase remains stable for at least three days. Thermal treatment at 100 K restores the PI phase to the LT phase due to the critical temperature of the phase transition from the PI phase to the LT phase at 70 K. Both the UV–vis spectra (Fig. S13†) and the $\chi_M T$–T plot (Fig. S16†) support this transition. PI magnetization is repeatedly observed (Fig. 6c).
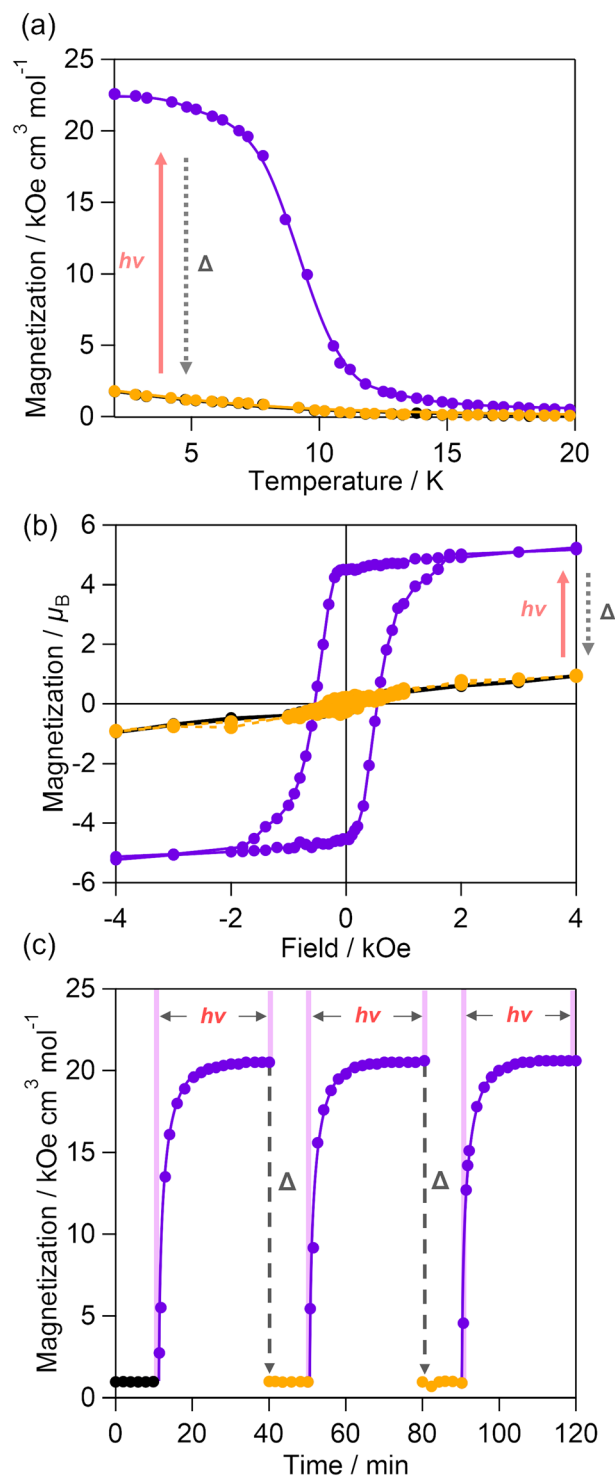

Fig. 6 Magnetic measurements of **CoWisoq** before and after photoirradiation and after thermal annealing. (a) Magnetization vs. temperature plots under 500 Oe. (b) Magnetization vs. magnetic field plots at 2 K in the range of −4 to 4 kOe. (c) Magnetization vs. time plots in the repeated photoirradiation and thermal annealing processes under 500 Oe. Black, purple, and yellow circles indicate before and after photoirradiation (980 nm, 26 mW cm^{-2}, 30 min) and after thermal annealing at 100 K, respectively.

2756 | *Inorg. Chem. Front.*, 2024, **11**, 2752–2762

This journal is © the Partner Organisations 2024

We then examined the photoresponsivity of the PI phase to confirm the photoreversibility from the PI phase to the LT phase using 473-, 532-, and 660 nm laser light. However, such a PI phase transition did not occur. To verify the ferromagnetic interaction between the Co^{II} and W^V in the PI phase, we measured the Faraday ellipticity after irradiation at low temperatures from 4 K to 80 K by applying a field of 10 kOe (Fig. 7, S7†). The Faraday ellipticities are attributed to the d–d transitions of Co^{II} at 460 and 550 nm. Additionally, the ligand-to-metal CT of W^V at 390 nm are parallel to each other, supporting the existence of a ferromagnetic interaction between Co^{II} and W^V.[62,63] Furthermore, the magnetic property of the PI phase of **CoWisoq** was precisely examined. The PI phase is stable up to 70 K. Fig. 8 plots the temperature and magnetic field dependences of the magnetization of the PI phase in
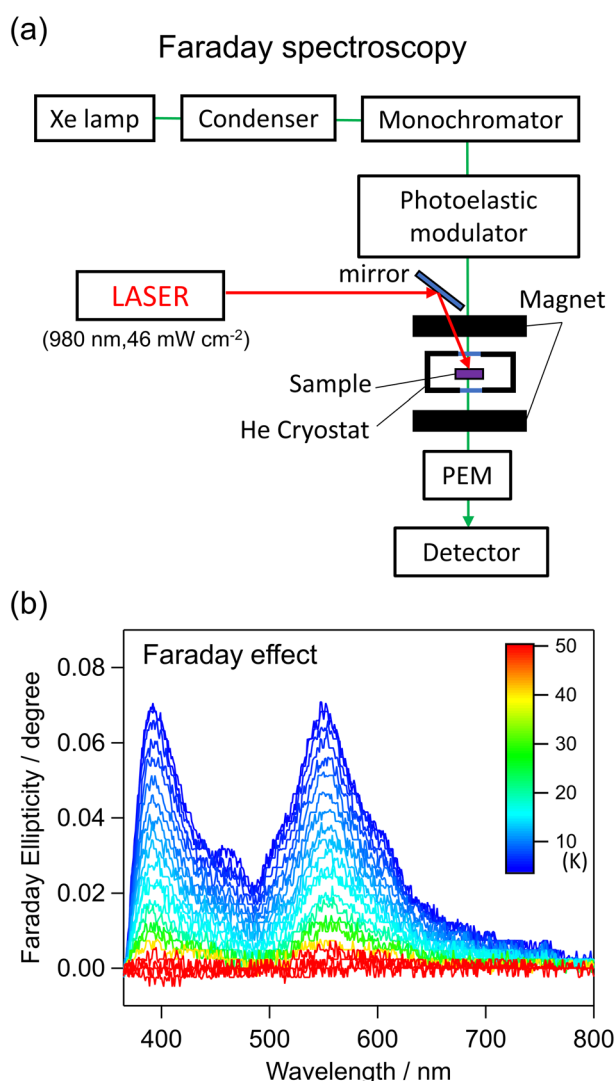

Fig. 7 Faraday ellipticity measurement of the PI phase in **CoWisoq**. (a) Set up of the photoinduced Faraday ellipticity measurement system. (b) Variable-temperature Faraday ellipticity of the PI phase in **CoWisoq** upon applying a magnetic field of 10 kOe in the range of 360 to 800 nm.
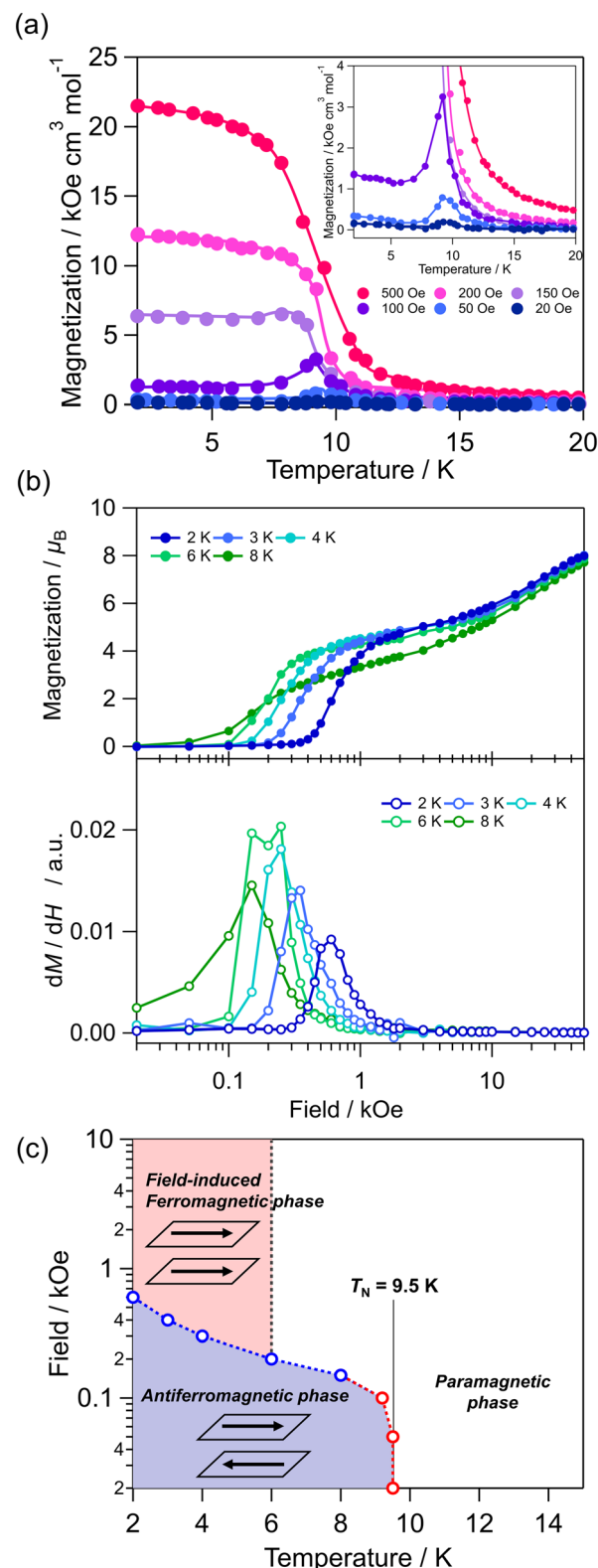

Fig. 8 (a) Magnetization *vs.* temperature curves of the PI phase under magnetic fields of 20, 50, 100, 150, 200, and 500 Oe. Inset shows an enlargement of the low-magnetization region. (b) Initial magnetization *vs.* magnetic field plots (upper) and the first derivative of the initial magnetization (d*M*/d*H*) (lower) of the PI phase at temperatures of 2, 3, 4, 6, and 8 K in the range of 0–50 kOe. (c) Magnetic field–temperature phase diagram for the PI phase of **CoWisoq**. T_N indicates the Néel temperature.

This journal is © the Partner Organisations 2024

Inorg. Chem. Front., 2024, **11**, 2752–2762 | **2757**

various conditions. The M–T curves in several external fields show spontaneous magnetizations under magnetic fields above 150 Oe and a small magnetization under magnetic fields below 100 Oe (Fig. 7a). The magnetic field dependences of the M–T curves indicate a spin-flip from an antiferromagnetic phase with a critical temperature like Néel temperature (T_N) to a magnetic field–induced ferromagnetic phase. The initial magnetization in the M–H plots from 2 K to 8 K presents remarkable increments of the magnetization in the range of 0.1–0.6 kOe (Fig. 7b), signifying a spin–flip phenomenon.[64–68] The spin–flip field (H_{ex}) is expressed by the first derivative of the initial M–H plots (dM/dH), and H_{ex} decreases upon heating. The temperature dependence of the H_{ex} values provides the H–T phase diagram for the PI phase of **CoWisoq** (Fig. 7c). **CoWisoq** exhibits a metamagnetic behavior. The M–H measurements in the range of −50 to 50 kOe at 2, 3, 4, 6, and 8 K indicate temperature dependences of Hc. The remnant magnetization disappears around 6 K. Additionally, the M–H plots above 6 K resemble the typical curve for metamagnetic behavior (Fig. S18 and S19†). Thus, the ferromagnetic ordering in the PI phase is preserved in a zero magnetic field below 6 K. Considering these results for the magnetic measurements and the structural analyses, the metamagnetic behavior of the PI phase can be explained as follows. The cyanido-bridged Co^{II}–W^V layer shows ferromagnetic ordering due to ferromagnetic interactions between Co^{II} and W^V, as supported by the saturation magnetization value and the Faraday ellipsometry. Therefore, the antiferromagnetic interactions between the ferromagnetically ordered layers should be responsible for the antiferromagnetic alignment in the small magnetic field below H_{ex}. In the magnetic field above H_{ex}, the magnetic moments are parallelly ordered between the layers, resulting in the magnetic field–induced ferromagnetic phase. The ferromagnetic phase can be maintained even in a zero magnetic field due to the existence of Hc. Consequently, **CoWisoq** has an interesting PI phase with metamagnetism, including the ferromagnetic, antiferromagnetic, and paramagnetic phases.

Conclusions

We synthesized a new photomagnet based on the cyanido-bridged Co–W assembly. **CoWisoq** has a two-dimensional layered structure with crystallographically independent Co (Co1 and Co2) and W sites. Both the Co1 and Co2 sites have four isoq and two cyanide ligands. However, the π–π interactions between the isoq ligands differ. Two of the four isoq ligands on the Co1 site make π–π interactions, while all four isoq ligands on the Co2 site form π–π interactions. Magnetic and UV–vis spectroscopic studies reveal a thermal phase transition between the HT phase with the $Co_3^{II}W_2^V$ state and the LT phase with the $Co_2^{III}Co^{II}W_2^{IV}$ state. The LT phase is derived from a CT-induced spin transition between the Co and W sites. Charge transfer occurs only on the Co1 and W sites since the Co1 site has a more flexible coordination environment

than that of the Co2 sites as Co1 has fewer π–π interactions. The LT phase of the present compound exhibits an intriguing MMCT absorption band in the NIR region due to the weak ligand fields on the Co sites composed of four isoq and two cyanide ligands, which differs from the cyanido-bridged Co–W compounds reported previously. Irradiation with 980 nm light to the MMCT absorption band of the LT phase produces the PI phase with $Co_3^{II}W_2^V$ due to the photoinduced CT-induced spin transition.

Interestingly, the PI phase shows a metamagnetic behavior in which the ferromagnetic and antiferromagnetic orderings can be controlled by the magnetic field. In the present system, we can choose the ferromagnetic PI phase when applying a magnetic field above 150 Oe or the antiferromagnetic PI phase when the magnetic field is below 100 Oe. Previous studies have not reported a photomagnetic system in which the ferromagnetically and antiferromagnetically ordered states are controlled by applying such a small magnetic field. Since photomagnetic properties are a representative feature of molecule-based magnets, the present study showcases a new aspect of photomagnets based on the cyanido-bridged metal assembly.

Experimental

Materials

Synthesis

[{Co(isoquinoline)$_4$}$_3${W(CN)$_8$}$_2$]·2EtOH (**CoWisoq**) in the crystal form was prepared by reacting 2 mL of a mixed solution of ethanol/H_2O (2 : 1) including $CoCl_2·6H_2O$ (0.300 mmol) and isoquinoline (1.200 mmol) with 2 mL of an aqueous solution containing $Cs_3[W(CN)_8]·2H_2O$ (0.200 mmol) inserting 20 mL of a buffer solution of ethanol/H_2O (1 : 1) at room temperature in a dark, using a slow diffusion method. After 2–3 weeks, purple plate crystals were obtained by filtering and washing with ethanol. They were kept in the air for several days. The composition of **CoWisoq** was determined by CHN elemental analyses, ICP-MS spectrometry, and TG measurement (Fig. S1†). Elemental analyses: calcd for $Co_3W_2C_{128}H_{96}N_{28}O_2$ (**CoWisoq** M_w = 2602.8): Co, 6.79%; W, 14.13%; C, 59.07%; H, 3.72%; N, 15.07%. Found: Co, 6.75%; W, 14.21%; C, 58.73%; H, 3.74%; N, 15.12%. IR spectra; cyanide stretching vibration: 2122 cm^{-1}, 2141 cm^{-1}, 2147 cm^{-1}, and 2160 cm^{-1}. CH stretching vibrations of isoquinoline: 2900 cm^{-1}, 2925 cm^{-1}, 2967 cm^{-1}, 2977 cm^{-1}, and 3059 cm^{-1} (Fig. S2†).[37–40,71] Raman spectrum; cyanide stretching vibration: 2137 cm^{-1} (Fig. S3†).[71]

Measurements

Elemental analyses were performed using standard microanalytical methods for C, H, and N, and ICP-MS (Agilent

2758 | *Inorg. Chem. Front.*, 2024, **11**, 2752–2762

This journal is © the Partner Organisations 2024

7700x) for Co and W. The TG properties were measured by a Rigaku Thermo plus Evo II TG8120. The magnetic properties were studied with a superconducting quantum interference device (SQUID) magnetometer (Quantum Design MPMS). The temperature-dependent magnetic susceptibility measurement was carried out under an externally applied magnetic field of 5000 Oe. The diamagnetic contributions from the samples were corrected on the basis of Pascal's constants.[72] Powder XRD measurements for **CoWisoq** at 293 K were performed using a Rigaku Miniflex diffractometer equipped with Cu Kα radiation (λ = 1.5406 Å). The diffraction patterns were recorded within a diffraction angle range of 5–70° in 0.02° steps and an exposure time of 1° min^{-1}. The infrared spectra at room temperature were measured by a spectrometer (JASCO FT/IR-4100). The measured samples were prepared by dispersing in KBr. The UV–vis spectrum at room temperature was measured using a spectrometer (JASCO V-670) and a sample dispersed in BaSO$_4$. Variable-temperature UV–vis absorption spectra were measured using a Shimadzu UV-3600 plus spectrometer with an Oxford Instruments Microstate-He cryostat and a continuous wave (cw) diode laser of 980 nm. The sample was prepared by dispersing in paraffin oil sandwiched between quartz plates. Photomagnetism measurements were conducted by SQUID. An optical fiber with its edge connected to the sample and a diode laser of 980 nm and 1064 nm were employed (Fig. S20 and S21†). The sample for the photomagnetic measurements was prepared with grided crystals which were sandwiched between tapes because **CoWisoq** was sufficiently stable without liquid paraffin to prevent evaporation of EtOH molecules in the crystal structure under the vacuum condition in the sample chamber of the magnetic measurement system. The Faraday effect measurement was conducted using a JASCO E250 type magneto-optical spectrometer with an Oxford Instruments Microstate-He cryostat and a cw diode laser of 980 nm. The sample was prepared by dispersing in paraffin oil sandwiched between CaF$_2$ plates. Single-crystal X-ray structures of **CoWisoq** at 300, 200, and 90 K were resolved on a Rigaku AFC10 diffractometer with a Rigaku Saturn Kappa CCD detector and a MicroMax-007 HF/VariMax rotating-anode X-ray generator. The single crystal was removed from the solution and placed inside the Paratone-N oil immediately. The crystal was placed on the cryoloop with a diameter of 100 μm and mounted on the diffractometer. The diffraction data were integrated after the experiment using Rigaku CrisAlisPro software. Crystal structures were solved by the direct method of SHELXS-97 program. Furthermore, using OLEX-2 1.5 software, these structures were refined and resolved to assign the missing electron density to the appropriate elements. The crystal structures at 90, 200, and 300 K are deposited in the Cambridge Crystallographic Data Centre of CCDC 2331970, 2331971, and 2331972,† respectively.

Calculation

Continuous shape measure analyses were performed using SHAPE software (version 2.1) to determine the geometry of eight-coordinated $[W(CN)_8]^{n-}$ (n = 3, 4) ions in **CoWisoq** at each temperature.[73]

Author contributions

K. Nakamura, K. Nakabayashi, and S. O. designed the study. K. Nakamura performed most of the experiments and analyzed the data. K. Nakamura and S. K. investigated photomagnetic measurements. K. Nakamura and K. Nakabayashi wrote the manuscript in discussion with all the authors.

Conflicts of interest

There are no conflicts to declare.

Acknowledgements

References

1 J. M. Manriquez, G. T. Yee, R. S. McLean, A. J. Epstein and J. S. Miller, A room-temperature molecular/organic-based magnet, *Science*, 1991, **252**, 1415–1417.

2 S. Ferlay, T. Mallah, R. Ouahes, P. Veillet and M. Verdaguer, A room-temperature organometallic magnet based on Prussian blue, *Nature*, 1995, **378**, 701–703.

3 L. Catala and T. Mallah, Nanoparticles of Prussian blue analogs and related coordination polymers: From information storage to biomedical applications, *Coord. Chem. Rev.*, 2017, **346**, 32–61.

4 E. Coronado and P. Day, Magnetic Molecular Conductors, *Chem. Rev.*, 2004, **104**, 5419–5448.

5 S. Ohkoshi, T. Iyoda, A. Fujishima and K. Hashimoto, Magnetic properties of mixed ferro-ferrimagnets composed of Prussian blue analogs, *Phys. Rev. B: Condens. Matter Mater. Phys.*, 1997, **56**, 11642–11652.

This journal is © the Partner Organisations 2024

Inorg. Chem. Front., 2024, **11**, 2752–2762 | **2759**

6 S. M. Holmes and G. S. Girolami, Sol–Gel Synthesis of $KV^{II}[Cr^{III}(CN)_6]\cdot 2H_2O$: A Crystalline Molecule-Based Magnet with a Magnetic Ordering Temperature above 100 °C, *J. Am. Chem. Soc.*, 1999, **121**, 5593–5594.

7 A. K. Bar, C. Pichon and J.-P. Sutter, Magnetic anisotropy in two- to eight-coordinated transition–metal complexes: Recent developments in molecular magnetism, *Coord. Chem. Rev.*, 2016, **308**, 346–380.

8 M. Kurmoo, Magnetic metal-organic frameworks, *Chem. Soc. Rev.*, 2009, **38**, 1353–1379.

9 S. J. Blundell and F. L. Pratt, Organic and molecular magnets, *J. Phys.: Condens. Matter*, 2004, **16**, R771–R828.

10 S. Ohkoshi, K. Imoto, Y. Tsunobuchi, S. Takano and H. Tokoro, "Light-induced spin-crossover magnet, *Nat. Chem.*, 2011, **3**, 564–569.

11 P. Perlepe, I. Oyarzabal, A. Mailman, M. Yquel, M. Platunov, I. Dovgaliuk, M. Rouzières, P. Négrier, D. Mondieig, E. A. Suturina, M.-A. Dourges, S. Bonhommeau, R. A. Musgrave, K. S. Pedersen, D. Chernyshov, F. Wilhelm, A. Rogalev, C. Mathonière and R. Clérac, Metal-organic magnets with large coercivity and ordering temperatures up to 242 °C, *Science*, 2020, **370**, 587–592.

12 S. Chorazy, J. J. Zakrzewski, M. Magott, T. Korzeniak, B. Nowicka, D. Pinkowicz, R. Podgajny and B. Sieklucka, Octacyanidometallates for multifunctional molecule-based materials, *Chem. Soc. Rev.*, 2020, **49**, 5945–6001.

13 K. Inoue, T. Hayamizu, H. Iwamura, D. Hashizume and Y. Ohashi, Assemblage and Alignment of the Spins of the Organic Trinitroxide Radical with a Quartet Ground State by Means of Complexation with Magnetic Metal Ions. A Molecule-Based Magnet with Three-Dimensional Structure and High T_C of 46 K, *J. Am. Chem. Soc.*, 1996, **118**, 1803–1804.

14 P. Gütlich, A. B. Gaspar, V. Ksenofontov and Y. Garcia, Pressure effect studies in molecular magnetism, *J. Phys.: Condens. Matter*, 2004, **16**, S1087.

15 S. Ohkoshi, T. Hozumi and K. Hashimoto, Design and preparation of a bulk magnet exhibiting an inverted hysteresis loop, *Phys. Rev. B: Condens. Matter Mater. Phys.*, 2001, **64**, 132404.

16 A. Bleuzen, C. Lomenech, V. Escax, F. Villain, F. Varret, C. C. dit Moulin and M. Verdaguer, Photo-induced Ferrimagnetic Systems in Prussian Blue Analogues $CI_xCo_4[Fe(CN)_6]_y$ (CI = Alkali Cation). 1. Conditions to Observe the Phenomenon, *J. Am. Chem. Soc.*, 2000, **122**, 6648–6652.

17 D. M. Pajerowski, M. J. Andrus, J. E. Gardner, E. S. Knowles, M. W. Meisel and D. R. Talham, Persistent Photo-induced Magnetism in Heterostructures of Prussian Blue Analogues, *J. Am. Chem. Soc.*, 2010, **132**, 4058–4059.

18 S. Ohkoshi and H. Tokoro, Photomagnetism in Cyano-Bridged Bimetal Assemblies, *Acc. Chem. Res.*, 2012, **45**, 1749–1758.

19 S. Ohkoshi, S. Takano, K. Imoto, M. Yoshikiyo, A. Namai and H. Tokoro, 90-degree optical switching of output second-harmonic light in chiral photomagnet, *Nat. Photonics*, 2013, **8**, 65–71.

20 M.-H. Zeng, Z. Yin, Y.-X. Tan, W.-X. Zhang, Y.-P. He and M. Kurmoo, Nanoporous Cobalt(II) MOF Exhibiting Four Magnetic Ground States and Changes in Gas Sorption upon Post-Synthetic Modification, *J. Am. Chem. Soc.*, 2014, **136**(12), 4680–4688.

21 J. Zhang, W. Kosaka, Y. Kitagawa and H. Miyasaka, A metal–organic framework that exhibits CO2-induced transitions between paramagnetism and ferrimagnetism, *Nat. Chem.*, 2021, **13**, 19–199.

22 J. Milon, M.-C. Daniel, A. Kaiba, P. Guionneau, S. Brandès and J.-P. Sutter, Nanoporous Magnets of Chiral and Racemic $[\{Mn(HL)\}_2Mn\{Mo(CN)_7\}_2]$ with Switchable Ordering Temperatures (T_C = 85 K ↔ 106 K) Driven by H_2O Sorption (L) N,N-Dimethylalaninol), *J. Am. Chem. Soc.*, 2007, **129**, 13872–13878.

23 S. Ohkoshi, K. Arai, Y. Sato and K. Hashimoto, Humidity-induced magnetization and magnetic pole inversion in a cyano-bridged metal assembly, *Nat. Mater.*, 2004, **3**, 857–861.

24 N. Yanai, W. Kaneko, K. Yoneda, M. Ohba and S. Kitagawa, Reversible Water-Induced Magnetic and Structural Conversion of a Flexible Microporous Ni(II)Fe(III) Ferromagnet, *J. Am. Chem. Soc.*, 2007, **129**, 3496–3349.

25 S. Chorazy, K. Nakabayashi, S. Ohkoshi and B. Sieklucka, Green to red luminescence switchable by excitation light in cyanido-bridged Tb^{III}–W^V ferromagnet, *Chem. Mater.*, 2014, **26**, 4072–4075.

26 S. Chorazy, B. Sieklucka and S. Ohkoshi, Near-Infrared Photoluminescence in Hexacyanid–Bridged Nd–Cr Layered Ferromagnet, *Cryst. Growth Des.*, 2016, **16**, 4918–4925.

27 J. A. DeGayner, I.-R. Jeon, L. Sun, M. Dincǎ and T. D. Harris, 2D Conductive Iron-Quinoid Magnets Ordering up to T_C = 105 K via Heterogenous Redox Chemistry, *J. Am. Chem. Soc.*, 2017, **139**, 4175–4184.

28 J. Zhang, W. Kosaka, Y. Kitagawa and H. Miyasaka, A Host–Guest Electron Transfer Mechanism for Magnetic and Electronic Modifications in a Redox-Active Metal–Organic Framework, *Angew. Chem., Int. Ed.*, 2022, **61**, 1–9.

29 S. Ohkoshi, K. Nakagawa, M. Yoshikiyo, A. Namai, K. Imoto, Y. Nagane, F. Jia, O. Stefanczyk, H. Tokoro, J. Wang, T. Sugahara, K. Chiba, K. Motodohi, K. Isogai, K. Nishioka, T. Momiki and R. Hatano, Giant adiabatic temperature change and its direct measurement of a barocaloric effect in a charge-transfer solid, *Nat. Commun.*, 2023, **14**, 8466.

30 T. Yoshida, K. Nakabayashi, H. Tokoro, M. Yoshikiyo, A. Namai, K. Imoto, K. Chiba and S. Ohkoshi, Extremely low-frequency phonon material and its temperature- and photo-induced switching effects, *Chem. Sci.*, 2020, **11**, 8989–8998.

31 S. Ohkoshi, K. Nakagawa, K. Tomono, K. Imoto, Y. Tsunobuchi and H. Tokoro, *J. Am. Chem. Soc.*, 2010, **132**, 6620–6621.

2760 | *Inorg. Chem. Front.*, 2024, **11**, 2752–2762

This journal is © the Partner Organisations 2024

32 R. Garde, C. Desplanches, A. Bleuzen, P. Veillet and M. Verdaguer, New Molecule-Based Magnets: From Hexacyano to Octacyanometalates, *Mol. Cryst. Liq. Cryst.*, 1999, **334**, 587–595.

33 P. M. Kiernan and W. P. Griffith, Studies on transition-metal cyano-complexes. Part I. Octacyanoniobates(III), -niobates(IV), -molybdates(V), and -tungstates(V), *J. Chem. Soc., Dalton Trans.*, 1975, 2489–2494.

34 T. S. Venkatakrishnan, S. Sahoo, N. Bréfuel, C. Duhayon, C. Paulsen, A.-L. Barra, S. Ramasesha and J.-P. Sutter, Enhanced Ion Anisotropy by Nonconventional Coordination Geometry: Single-Chain Magnet Behavior for a [{$Fe^{II}L$}$_2${$Nb^{IV}(CN)_8$}] Helical Chain Compound Designed with Heptacoordinate Fe^{II}, *J. Am. Chem. Soc.*, 2010, **132**, 6047–6056.

35 S. Chorazy, M. Rams, A. Hoczek, B. Czarnecki, B. Sieklucka, S. Ohkoshi and R. Podgajny, Structural anisotropy of cyanide-bridged {$Co^{II}_9W^V_6$} single-molecule magnets induced by bidentate ligands: towards the rational enhancement of an energy barrier, *Chem. Commun.*, 2016, **52**, 4772–4775.

36 Y. Arimoto, S. Ohkoshi, Z. J. Zhong, H. Seino, Y. Mizobe and K. Hashimoto, Photo-induced magnetization in a two-dimensional cobalt octacyanotungstate, *J. Am. Chem. Soc.*, 2003, **125**, 9240–9241.

37 S. Ohkoshi, Y. Hamada, T. Matsuda, Y. Tsunobuchi and H. Tokoro, Crystal structure, charge-transfer-induced spin transition, and photoreversible magnetism in a cyano-bridged cobalt-tungstate bimetallic assembly, *Chem. Mater.*, 2008, **20**, 3048–3054.

38 N. Ozaki, H. Tokoro, Y. Hamada, A. Namai, T. Matsuda, S. Kaneko and S. Ohkoshi, Photo-induced magnetization with a high Curie temperature and a large coercive field in a Co–W bimetallic assembly, *Adv. Funct. Mater.*, 2012, **20**, 2089–2093.

39 Y. Miyamoto, T. Nasu, N. Ozaki, Y. Umeta, H. Tokoro, K. Nakabayashi and S. Ohkoshi, Photo-induced magnetization and first-principles calculations of a two-dimensional cyanide-bridged Co–W bimetal assembly, *Dalton Trans.*, 2016, **45**, 19249–19256.

40 K. Nakamura, K. Nakabayashi, K. Imoto and S. Ohkoshi, Room-temperature bistability in a cobalt octacyanidotungstate framework showing a charge-transfer phase transition with a red-blue color change, *Inorg. Chem. Front.*, 2023, **10**, 850–859.

41 R. J. Deeth, D. L. Foulis and B. J. Williams-Hubbard, Molecular mechanics for multiple spin states of transition metal complex, *Dalton Trans.*, 2003, 3949–3955.

42 T. Ishii, S. Tsuboi, G. Sakane, M. Yamashita and B. K. Breedlove, Universal spectrochemical series of six-coordinate octahedral metal complexes for modifying the ligand field splitting, *Dalton Trans.*, 2009, 680–687.

43 J. Titis, J. Hudak, J. Kozisek, A. Krutosikova, J. Moncol, D. Tarabova and R. Boca, Structural, spectral and magnetic properties of carboxylato cobalt(II) complexes with heterocyclic N-donor ligands: Reconstruction of magnetic parameters from electronic spectra, *Inorg. Chim. Acta*, 2012, **388**, 106–113.

44 T. Oguma, D. Tsuneda, Y. Tsutsumi, Y. Fujikawa, M. Nakano, T. Ishii, G. Sakane and K. Ogasaware, The magnetism change by Jahn-Teller distortion in octahedral hexa-coordinate complex, *IOP Conf. Ser.: Mater. Sci. Eng.*, 2020, **835**, 012014.

45 R.-M. Wei, M. Kong, F. Cao, J. Li, T.-C. Pu, L. Yang, X.-L. Zhang and Y. Song, Water induced spin-crossover behaviour and magneto-structural correlation in octacyano-tungstate(IV)-based iron(II) complexes, *Dalton Trans.*, 2016, **45**, 18463–18652.

46 J. Qian, H. Yoshikawa, J. Hu, M. G. Humphrey, J. Zhang, K. Awaga and C. Zhang, Auxiliary ligand-induced structural diversities of octacyanometalate-based heterobimetallic coordination polymers towards diverse magnetic properties, *Dalton Trans.*, 2019, **48**, 7666–7676.

47 F. Setifi, A. Ota, L. Ouahab, S. Golhen, H. Yamochi and G. Saito, Charge Transfer Salts of BO with Paramagnetic Isothiocyanato Complex Anions: (BO)[M(isoq)$_2$(NCS)$_4$]; M=Cr^{III} or Fe^{III}, isoq = isoquinoline and BO=Bis(ethylene-dioxo)tetrathiafulvalene, *J. Solid State Chem.*, 2002, **168**, 450–456.

48 Y. Meng, Q. Q. Sheng, Md. N. Hoque, Y.-C. Chen, S.-G. Wu, J. Tucek, R. Zboril, T. Liu, Z.-P. Ni and M.-L. Tong, Two-Step Spin-Crossover with Three Inequivalent Fe^{II} Sites in a Two-Dimensional Hofmann-Type Coordination Polymer, *Chem. – Eur. J.*, 2017, **23**, 10034–10037.

49 J. C. Rendón-Balboa, L. Villanueva-Sánchez, L. D. Rosales-Vázquez, J. Valdes-García, A. R. Vilchis-Nestor, D. Martínez-Otero, S. Martínez-Vargas and A. Dorazco-González, Structure of a luminescent 3D coordination polymer constructed with a trinuclear core of cadmium-trimesate and isoquinoline, *Inorg. Chim. Acta*, 2018, **483**, 235–240.

50 S. Alvarez, A cartography of the van der Waals territories, *Dalton Trans.*, 2013, **42**, 8617–8636.

51 C. Janiak, A critical account on π-π stacking in metal complexes with aromatic nitrogen-containing ligands, *J. Chem. Soc., Dalton Trans.*, 2000, 3885–3896.

52 F. Lloret, M. Julve, J. Cano, R. Ruiz-Garcia and E. Pardo, Magnetic properties of six-coordinated high-spin cobalt(II) complexes: Theoretical background and its application, *Inorg. Chim. Acta*, 2008, **361**, 3432–3445.

53 S. M. Ostrovsky, K. Falk, J. Pelikan, D. A. Brown, Z. Tomkowicz and W. Haase, Orbital Angular Momentum Contribution to the Magneto-Optical Behavior of a Binuclear Cobalt(II) Complex, *Inorg. Chem.*, 2006, **45**, 688–694.

54 K. Nakabayashi, S. Chorazy, D. Takahashi, T. Kinoshita, B. Sieklucka and S. Ohkoshi, Cesium Cyano-Bridged Co^{II}–M^V (M = Mo and W) Layered Frameworks Exhibiting High Thermal Durability and Metamagnetism, *Cryst. Growth Des.*, 2014, **14**, 6093–6100.

55 S. Chorazy, K. Nakabayashi, K. Imoto, J. Mlynarski, B. Sieklucka and S. Ohkoshi, Conjuction of chirality and slow magnetic relaxation in the supermolecular network

This journal is © the Partner Organisations 2024

Inorg. Chem. Front., 2024, **11**, 2752–2762 | **2761**

constructed of crossed cyano-bridged Co^{II}-W^V molecular chains, *J. Am. Chem. Soc.*, 2012, **134**, 19989–19992.

56 D. M. L. Goodgame, M. A. Hitchman, D. F. Marsham and C. E. Souter, Complexes of Cobalt(II) Nitrite with Amine Ligands, *J. Chem. Soc. A*, 1969, 2464–2468.

57 B. J. A. Kakazal and G. A. Melson, Aromatic Diamine Complexes, II. Tetragonal Distortion in some Cobalt(II) Complexes, *Inorg. Chim. Acta*, 1970, **4**, 360–364.

58 R. W. Matthews, A. D. Hamer, D. L. Hoof, D. G. Tisley and R. A. Walton, Study on metal carboxylates. Part IV. Pyridine-2,6-dicarboxylate complexes of cobalt(II), nickel(II), rhodium(II), and rhodium(III). Synthesis, spectral and magnetic properties, and a study of rhodium 3d binding energies by X-ray photoelectron spectroscopy, *J. Chem. Soc., Dalton Trans.*, 1973, **10**, 1035–1038.

59 E. Ochiai, K. M. Long, C. R. Sperati and D. H. Busch, Bonded Organic Derivatives of a Cobalt(III) Macrocyclic Complex, *J. Am. Chem. Soc.*, 1969, **91**(12), 3201–3206.

60 P. O. Whimp and N. F. Curtis, Some cyclic tetra-amines and their metal-ion complexes. Part V. Cobalt(III) complexes of two isomeric 5,7,7,12,12,14-hexamethyl-1,4,8,11-tetra-azacyclotetradecanes, *J. Chem. Soc. A*, 1968, 188–190.

61 A. B. P. Lever, *Inorganic Chemistry Spectroscopy*, 1968.

62 Y. Sato, S. Ohkoshi and K. Hashimoto, Photo-induced Faraday effect in a cobalt-iron polycyanide film, *J. Appl. Phys.*, 2002, **92**(8), 4834–4836.

63 M. Ohba, T. Iwamoto and H. Okawa, Magneto-optical Properties of Two-dimensional Cyanide-Bridged $M^{III}Ni^{II}$ Bimetallic Assemblies (M=Fe, Co), *Chem. Lett.*, 2002, **10**, 1046–1047.

64 W. Kosaka, M. Itoh and H. Miyasaka, Metamagnetism with $T_N = 97$ K in a layered assembly of paddlewheel [Ru$_2$] units and TCNQ: an empirical rule for interlayer distances deter-mining the magnetic ground state, *Mater. Chem. Front.*, 2018, **2**, 497–504.

65 J. Mandal, P. Brandão, S. Benmansour, C. J. Gómez-García and A. Saha, First Example of Chromone-Based Nickel(II) Coordination Polymers with Tunable Magnetic Properties, *Cryst. Growth Des.*, 2022, **22**, 7544–7554.

66 S. Kaneko, Y. Tsunobuchi, S. Sakurai and S. Ohkoshi, Two-dimensional metamagnet composed of a cesium copper octacyanotungustate, *Chem. Phys. Lett.*, 2007, **446**, 292–296.

67 S. Ohkoshi, Y. Arimoto, T. Hozumi, H. Seino, Y. Mizobe and K. Hashimoto, Two-dimensional metamagnet composed of cyano-bridged Cu^{II}-W^V bimetallic assembly, *Chem. Commun.*, 2003, **22**, 2772–2773.

68 S. Chorazy, R. Podgajny, A. M. Majcher, W. Nitek, M. Rams, E. A. Suturina, L. Ungur, L. F. Chibotaru and B. Sieklucka, Magnetic anisotropy of Co^{II}-W^V ferromagnet: single crystal and *ab initio* study, *CrystEngComm*, 2013, **15**, 2378–2385.

69 J. G. Leipoldt, L. D. C. Bok and P. J. Cilliers, The preparation of potassium octacyanotungstate(IV) dihydrate, *Z. Anorg. Allg. Chem.*, 1974, **407**, 350–352.

70 L. D. C. Bok, J. G. Leipoldt and S. S. Basson, The preparation of Cs$_3$Mo(CN)$_8$·2H$_2$O and Cs$_3$W(CN)$_8$·2H$_2$O, *Z. Anorg. Allg. Chem.*, 1975, **415**, 81–83.

71 M. Bolboaca, W. Kiefer and J. Popp, Fourier transform Raman and surface-enhanced Raman spectroscopy of some quinoline derivatives, *J. Raman Spectrosc.*, 2002, **33**, 207–212.

72 G. A. Bain and J. F. Berry, Diamagnetic Corrections and Pascal's Constants, *J. Chem. Educ.*, 2008, **85**, 532–536.

73 M. Llunell, D. Casanova, J. Cirera, J. Bofill, P. Alemany, S. Alvarez, M. Pinsky and D. Avnir, *SHAPE v. 2.1. Program for the Calculation of Continuous Shape Measures of Polygonal and Polyhedral Molecular Fragments*, University of Barcelona, Barcelona, Spain, 2013.

2762 | *Inorg. Chem. Front.*, 2024, **11**, 2752–2762

This journal is © the Partner Organisations 2024